Article

Density Functional Theory and Machine Learning Description and Prediction of Oxygen Atom Chemisorption on Platinum Surfaces and Nanoparticles

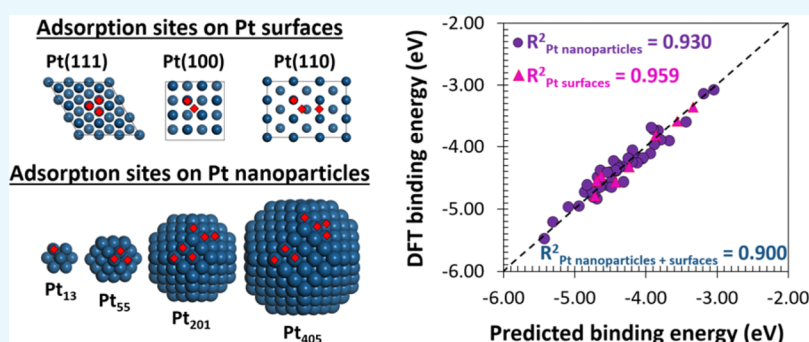David S. Rivera Rocabado, Yusuke Nanba, and Michihisa Koyama*

Read Online

ACCESS | Metrics & More | Article Recommendations

ABSTRACT: Elucidating chemical interactions between catalyst surfaces and adsorbates is crucial for understanding surface chemical reactivity. Herein, interactions between O atoms and Pt surfaces and nanoparticles are described as a linear combination of the properties of pristine surfaces and isolated nanoparticles. The energetics of O chemisorption onto Pt surfaces were described using only two descriptors related to surface geometrical features. The relatively high coefficient of determination and low mean absolute error between the density functional theory-calculated and predicted O binding energies indicate good accuracy of the model. For Pt nanoparticles, O binding is described by the geometrical features and electronic properties of isolated nanoparticles. Using a linear combination of five descriptors and accounting for nanoparticle size effects and adsorption site types, the O binding energy was estimated with a higher accuracy than with conventional single-descriptor models. Finally, these five descriptors were used in a general model that decomposes O binding energetics on Pt surfaces and nanoparticles. Good correlation was achieved between the calculated and predicted O binding energies, and model validation confirmed its accuracy. This is the first model that considers the nanoparticle size effect and all possible adsorption sites on Pt nanoparticles and surfaces.

■ INTRODUCTION

In the cathode environment of a polymer electrolyte fuel cell, O_2 is activated by proton and electron transfer to form OOH before O−O bond dissociation can occur.[1] Following OOH dissociation, the electrocatalyst should bind O and OH with moderate strength in order for the ensuing H_2O formation and desorption to be rapid; alternatively, the active sites will be covered by these species and will become inactive for O_2 dissociation. The energies of the O atom and OH adsorption onto various metals exhibit a linear scaling relationship with the limiting potential.[2] Experimental and density functional theory (DFT) results suggest that a surface capable of binding the O atom with a stability that is up to 0.4 eV lower than Pt(111) should exhibit enhanced activity for the oxygen reduction reaction (ORR) compared to Pt.[1,3] Thus, it is essential to determine the suitable descriptors of the energetics of adsorbent−adsorbate interactions to predict catalytic activity trends. In recent years, the DFT method has been recognized as a useful tool for understanding adsorbate−adsorbent interactions. Among the theory-based activity predictors, the Hammer−Nørskov model[4] linearly scales the d-band center and adsorption energy. Although the d-band center model displays a moderate linear correlation with the heats of adsorption of small molecules, such as CO, H_2, O_2, and C_xH_y, on various metal surfaces,[5] a close linear relationship for H_2, CO, and OH adsorption energies on Pt atoms supported on strained graphene,[6] good linearity for O binding energy on Rh surfaces,[7] and a close linear fit of CO and O atom binding energies on various metal surfaces,[8] only a
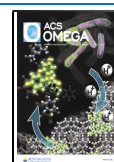
modest fit has been observed between the adsorption energy of an O atom on Pt and Pt alloy surfaces and their *d*-band centers.[9] Large deviations have been reported between adsorption energies and *d*-band centers for CO and O atoms adsorbed on Au surfaces and Au₁₂ nanoparticles.[10] It has been established that the relationship between adsorption energy and the *d*-band center does not account for the effect of low coordinated atoms, such as those located at the vertices and ridges of nanoparticles, especially in small cluster particles that do not expose well-defined planes.[11−13] Hence, when considering the variation in particle size and coordination of the adsorption site, the *d*-band center would not be suitable as the sole descriptor of the adsorption energy.[11] In search of new descriptors of adsorption energy, the generalized coordination number (GCN) has been shown to be more appropriate than the *d*-band center for rationalizing O, O_2, OOH, H_2O, and H_2O_2 adsorption on the top site of Pt nanoparticles.[14] Although machine learning has been used to describe CO adsorption on Pt nanoparticles as a linear combination of various descriptors, only the top site was considered as the adsorption site.[15] To address these limitations, a more robust and complete model has been proposed using supervised learning to describe the adsorption energy between NO and 4*d*- and 5*d*-transitions metals, considering top, bridge, and hollow adsorption sites.[16] Similarly, supervised learning was used to describe interactions between O atoms and bimetallic nanoparticles with a Pt skin configuration using an element-based GCN.[17] In this study, a multidescriptor model composed of the structural and electronic properties of Pt nanoparticles and Pt surfaces was implemented to estimate the O binding energy using multiple regression analysis, a machine learning algorithm. First, a model describing O binding to Pt surfaces alone was obtained using a linear combination of two surface geometrical features. The model exhibited an excellent linear correlation with the calculated O binding energy. Next, the O binding energy on Pt nanoparticles alone was predicted using a linear combination of five structural and electronic properties of the isolated nanoparticles. Model validation indicated that the model is robust and accurate for describing O binding to all the adsorption sites of differently sized Pt nanoparticles. The proposed descriptors were selected based on geometrical, electronic, and stability features of the isolated Pt nanoparticles, which have been reported elsewhere.[18] Finally, a model that can accurately decompose and estimate the O binding energy on Pt surfaces and nanoparticles, considering, for the first time, the nanoparticle size effect and the various adsorption sites of Pt nanoparticles and Pt surfaces, was obtained using the same descriptors as in the case of O binding to Pt nanoparticles alone. The DFT-calculated and predicted O binding energies exhibited a significant linear correlation. Model validation confirmed its accuracy in predicting the O binding energy on Pt nanoparticles of different sizes and on Pt surfaces. In all cases, the multi-descriptor model predicted O binding more accurately than the conventional single-descriptor models.

■ COMPUTATIONAL DETAILS

All calculations performed in this study were based on the plane wave DFT method implemented in the Vienna Ab initio Simulation Package (VASP 5.3.5).[19−21] Perdew−Burke−Ernzerhof parametrization under generalized gradient approximation was employed as the exchange-correlation functional together with the projector-augmented wave method.[22] Spin-

polarized calculations were performed throughout the study with a plane wave cutoff energy of 400 eV for nanoparticles and 600 eV for Pt surfaces. The convergence criteria for all calculations were set as the point at which the difference in the total energy between the two ionic steps was less than 10^{-4} eV/atom and 10^{-5} eV/atom for self-consistent field iterations. Optimization of the face-centered cubic (FCC) phase of bulk Pt was performed with $21 \times 21 \times 21$ Monkhorst-Pack k-point meshes for the Brillouin zone integration, wherein all the atoms and the entire crystal volume were relaxed. Following optimization, the calculated lattice parameters of bulk Pt, $a = 3.966$ Å, correlated well with the experimentally reported value of 3.916 Å.[23] To estimate the O binding energy on Pt surfaces, Pt(111), Pt(100), and Pt(110) were modeled with six, seven, and nine atomic Pt layers, respectively. While the optimization of the Pt(111) and Pt(100) surfaces was performed with a $6 \times 6 \times 1$ Monkhorst−Pack k-point mesh, a $4 \times 6 \times 1$ Monkhorst−Pack k-point mesh was employed for Brillouin zone integration during the optimization of Pt(110). The atoms of the three bottom layers of Pt(111) and Pt(100) and those of the four bottom layers of Pt(110) were frozen. The Pt surface models are shown in Figure 1a. Pt nanoparticles of
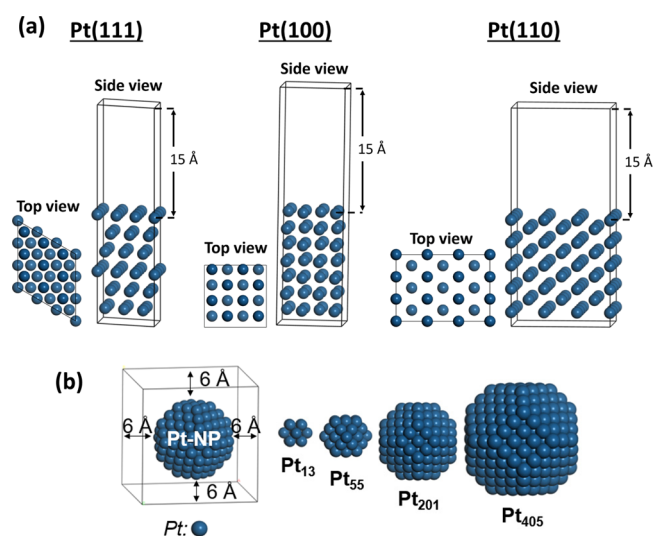

Figure 1. Models of (a) Pt surfaces and (b) Pt nanoparticles.

varying sizes containing 13, 55, 201, and 405 atoms were modeled and optimized. To avoid interactions between periodic images, the minimum distance between the cell boundaries and Pt atoms was set to 6 Å, that is, a minimum of 12 Å between neighboring image Pt nanoparticles. Pt nanoparticle models are shown in Figure 1b. Nanoparticle optimization was performed at the Γ point in reciprocal space, owing to the significant spatial extent of the systems, wherein all the Pt atoms were allowed to relax. The binding energy between O and Pt surfaces (E_{Pt_s}) and Pt nanoparticles (E_{Pt_n}), E_{bind}, was calculated as

$$E_{bind} = E_{Pt_{s/n}+O} - E_{Pt_{s/n}} - E_O \tag{1}$$

where $E_{Pt_{s/n} + O}$, $E_{Pt_{s/n}}$, and E_O denote the total energy of the O atom interaction with the Pt surface or Pt nanoparticle, that of the pristine Pt surface or isolated Pt nanoparticles, and that of the O atom, respectively. Using this definition of binding energy, negative values denote a more stable interaction of

between the O atom and the Pt nanoparticles/surfaces. During the geometry optimization of the O binding to Pt surfaces and nanoparticles, the same constraints were set for the Pt atom motion as in the case of the pristine/isolated surfaces/nanoparticles; only the atoms of the three bottom layers of Pt(111) and Pt(100) and those of the four bottom layers of Pt(110) were frozen, and for the nanoparticles, all atoms were allowed to relax. Bond order analysis was performed using the sixth generation density-derived electrostatic and chemical (DDEC6) method.[24] In statistical data analysis, multiple competing models are often considered. Akaike's information criterion (AIC) estimates the accuracy (the relative amount of information lost) and simplicity of the model by including a penalty for each descriptor used to estimate a dependent variable.[25] Thus, minimizing the AIC facilitates the selection of a model that is not overfitted and is close to optimal.[26] However, the AIC may become inaccurate for small sample sizes, especially when the ratio between the data sample and the number of descriptors is less than 40.[27] In such cases, the corrected AIC (AIC$_C$) should be used. In regression models, the definition of AIC$_C$ is as follows:[28]

$$AIC_C = 2k + n \ln\left\{ \frac{\sum_{i=1}^{n} [E_{bind_i} - \hat{E}_{bind_i}(x_i)]^2}{n} \right\} + \frac{2k(k+1)}{n-k-1} \tag{2}$$

where k, n, E_{bind}, and $\hat{E}_{bind}(x_i)$ are the number of descriptors in the model, the total number of samples, and DFT-calculated and predicted values of the O binding energy, respectively.

RESULTS AND DISCUSSION

O Binding on Pt Surfaces and Pt Nanoparticles. Figure 2 shows the adsorption sites and binding energies of O atoms
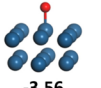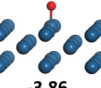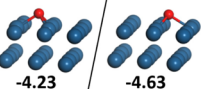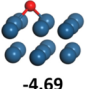

	Pt(111)	Pt(100)	Pt(110)
Top	-3.34	-3.56	-3.86
HCP/FCC	-4.23 / -4.63		
Bridge		-4.69	-4.43 / -4.72
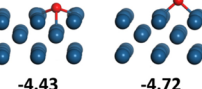
Figure 2. Adsorption sites and binding energies (eV) of O atom interactions on Pt surfaces.

on Pt surfaces. The preferred adsorption sites for the O atom on Pt(100) and Pt(110) surfaces are the bridge sites. A local minimum was not found for the interaction between the O atom and the bridge sites of Pt(111); the O atom moved to the threefold coordinated sites after optimization, which agrees with experimental observations showing that the most favorable adsorption site for the O atoms is the FCC.[29] From the calorimetric heats of the O adsorption on Pt(111), the Pt−O bond energy is estimated to be −4.32 eV,[30] which is in good agreement with our calculated values −4.23 and −4.63

eV for the O binding on the hexagonal close-packed (HCP) and FCC sites, respectively. The experimental value of the Pt−O distance, 2.01 ± 0.05 Å,[31] corresponds well with our calculated interatomic distance of the O interacting at the FCC and HCP sites (2.042 Å). For O binding to Pt(100) and Pt(110), no local minimum was found for the O atom chemisorption onto the HCP/FCC sites. Thermodynamic stability of the interaction between O and the top sites of the Pt surfaces decreased in the following order: Pt(110) > Pt(100) > Pt(111). When O interacts at the bridge site, the Pt(110) surface stabilizes the O binding to a greater extent than Pt(100). For Pt(110), a unique O binding occurs; the O atom interacts at the bridge position between two Pt atoms on the surface and on top of one Pt atom in the subsurface. The binding energy for this configuration is −4.43 eV. The O adsorption sites and their respective binding energies are shown in Figure 2. For Pt nanoparticle binding, the strength of O atom interaction decreases as the nanoparticle size increases. O binding preferentially occurs at the bridge sites, followed by threefold coordinated sites (FCC and HCP) and then the top sites of the Pt nanoparticles. When considering nanoparticles of the same size, the O atom interaction on a similar adsorption site is affected by the coordination of the Pt atoms composing the adsorption site. The O atom interaction with the Pt atoms in nanoparticles is more stable on under-coordinated atoms. The coordination number of the Pt atoms increases in the following order: atoms at the vertices have fewer coordinated atoms compared with atoms at the ridges, followed by atoms at the {100} and {111} facets. As shown in Figure 3, when the O atom is adsorbed on the top sites of Pt$_{201}$, the O binding energy decreases in the following order: top of the {111} facet > top of the {100} facet > top of the ridge atoms > top of a vertex atom. As the nanoparticle size increases, new adsorption sites comprising atoms with different coordination numbers become available; thus, it is difficult to determine the size effect from the adsorption site effect. The O binding energies for Pt$_{55}$ and Pt$_{201}$ are in good agreement with the previously reported values.[11] To the best of our knowledge, there are no experimental reports of the Pt−O bond energy for Pt nanoparticles. It should be noted that our calculations represent the O binding to isolated nanoparticles in vacuum and do not consider the effect of support, liquid environment, external voltage cycling, and so on, to which Pt nanoparticles are exposed during the fuel cell operation. Thus, a direct comparison cannot be made. However, the stability trend of the O interaction as a function of the adsorption site coordination, that is, more stable Pt−O interaction for the Pt atoms at vertices, then edges, Pt(111), and Pt(100), is reproduced for the O$_2$ dissociation on tetrahedral (4.8 ± 0.1 nm), cubic (7.1 ± 0.2 nm), and "near-spherical" (4.9 ± 0.1 nm) Pt nanoparticles[32] and is in agreement with Monte Carlo simulations of the O interaction on Pt$_{489}$.[33] Although, elucidating the size effect experimentally is a difficult task because the activity of catalysts is approximated by the turnover frequencies, which are quantities averaged over the different sizes and active sites of the nanoparticles;[11] the general trend for the ORR is that as the size of the nanoparticle increases, the activity increases due to weaker binding of oxygenated species.[11,34,35] When comparing the O binding energies on the same adsorption site of the different Pt nanoparticles in this study, it can be seen that the O interaction decreases with the increasing nanoparticle size.
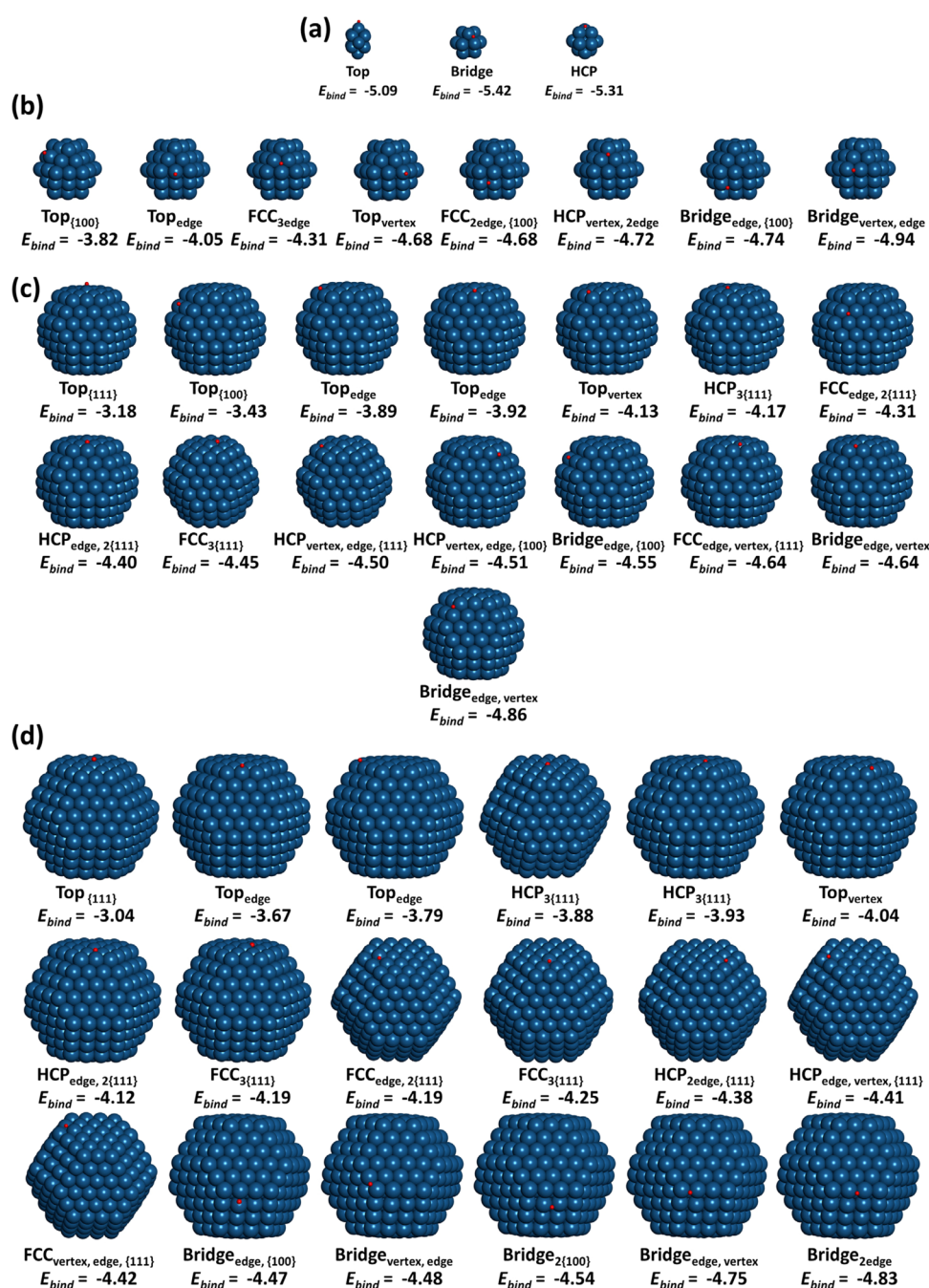
Figure 3. O adsorption sites and binding energies (eV) on (a) Pt_{13}, (b) Pt_{55}, (c) Pt_{201}, and (d) Pt_{405}.

Multiple Description Analysis of the O Binding Energy. Figure 4 shows the linear relationships between the calculated O binding energy and the conventional adsorption descriptors, namely, the d-band center (Figure 4a) and the GCN (Figure 4b). An extremely low coefficient of determination (R^2) of 0.040 was observed between the O binding energies on Pt surfaces and the d-band centers. The degree of discrepancy between the predicted and observed values is approximated by the mean absolute error (MAE). The MAE for the O binding to Pt surfaces and the values predicted by the d-band center is 0.421 eV. Considering the relationship between the O binding energy on Pt nanoparticles alone and the d-band center, an improved linear correlation was observed, where $R^2 > 0.500$ when each adsorption site (top, bridge, and FCC/HCP) was considered separately, and when

all the nanoparticle adsorption sites were considered, an R^2 value of 0.331 was obtained, and the MAE decreased to 0.317 eV. However, when all the adsorption sites were included (Pt nanoparticles and Pt surfaces), R^2 decreased to 0.254, and the MAE increased to 0.346 eV, demonstrating that the d-band center alone could not explain the chemisorption of O atoms on a combination of Pt nanoparticles and Pt surfaces. Figure 4b shows that the GCN exhibits a better linear relationship with the O binding energy on Pt surfaces than the d-band center; however, the R^2 value was also low (0.102) and the MAE large (0.449 eV). When only the Pt nanoparticles were considered, the R^2 value between the O binding energy and the GCN of the various adsorption sites ranged from 0.666 for the FCC/HCP sites to 0.719 for the bridge sites and up to 0.879 for the interaction of O atoms with the top sites of Pt
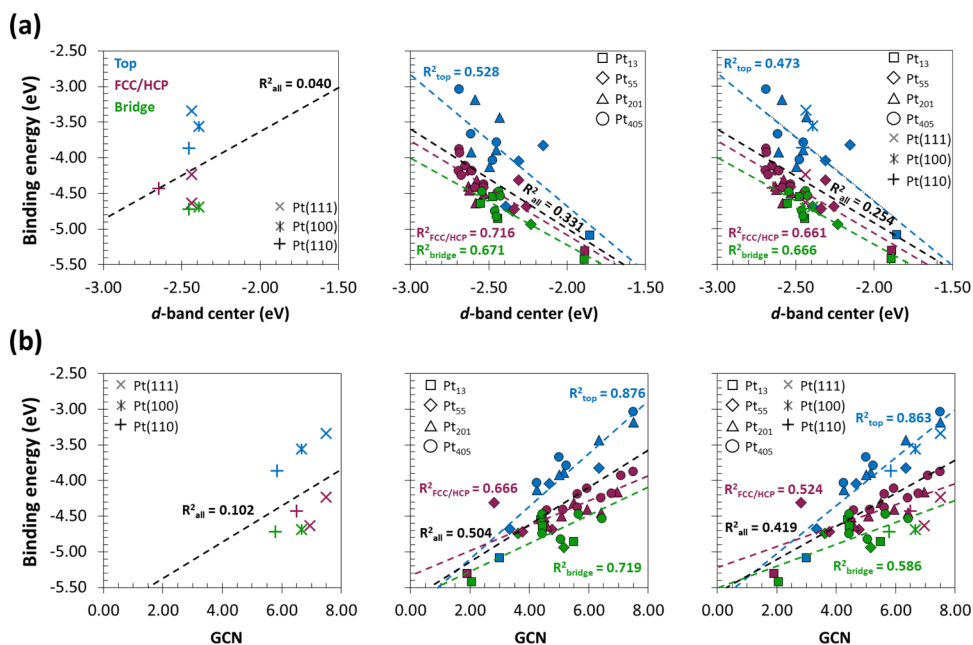
Figure 4. O binding energy relationship with (a) d-band center and (b) GCN of Pt surfaces, Pt nanoparticles, and a combination of the two. Linear regression lines and coefficients of determination are also shown.
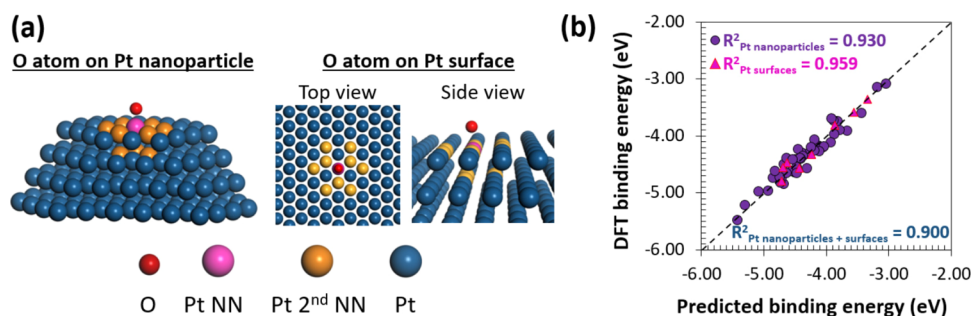

Figure 5. (a) Schematics of the NN and 2nd NN of the adsorption site on Pt surfaces and Pt nanoparticles and (b) relationship between the DFT-calculated and predicted O binding energies on Pt surfaces only, Pt nanoparticles only, and Pt surfaces and nanoparticles combined. Linear regression lines and coefficients of determination are shown.

nanoparticles. Nevertheless, R^2 was slightly larger than 0.500 when all nanoparticle adsorption sites were considered. The magnitude of the dissimilarities between the DFT-calculated and the GCN-predicted O binding energies is 0.287 eV. The linear relationship between the O binding energies on Pt nanoparticles and Pt surfaces with the GCN of each adsorption site decreased considerably for the bridge and FCC/HCP sites, providing R^2 values that were even lower than the correlation with the d-band center. When all the Pt nanoparticle and Pt surface adsorption sites were considered, the R^2 value of the linear relationship between the GCN and O binding energy was 0.419, with an MAE of 0.314 eV. Thus, the d-band center and the GCN cannot be considered as the sole descriptor of the O binding energy on Pt surfaces or Pt nanoparticles alone or on a combination of the two. To overcome this challenge, in this study, the O binding energy is described as a linear combination of several descriptors (before O binding) using multiple regression analysis. The descriptors associated with the O binding energy were selected from among 20 descriptors related to the geometrical features and electronic properties of the nearest neighbors (NN) and second nearest neighbors (2nd NN) of the adsorption site. The four geometrical features considered are the GCN, the average Pt−Pt distance of the

NN, the average Pt−Pt distance of the NN + 2nd NN, and the size of the nanoparticle approximated by $n^{-1/3}$ (n = number of atoms in the nanoparticle). From the 16 electronic properties, 8 correspond to the charge, the sum of bond orders, the s-, p-, and d-band centers, and the s-, p-, and d-bandwidths of the NN of the adsorption site, and the remaining 8 correspond to the same properties but for the NN + 2nd NN. To make a direct comparison, these electronic properties were obtained after a self-consistent field calculation using the same computational details as for the geometry optimization. Charge and bond orders were obtained using the DDEC6 method. The definitions of NN and NN + 2nd NN of the adsorption site are shown in Figure 5a. There are new methods for identifying descriptors for materials' properties, such as the one implemented in the sure independence screening and sparsifying operator algorithm.[36] In this study, the model describing the O binding to surfaces and nanoparticles is obtained from linear combinations of the pristine/isolated surfaces/nanoparticles before their interaction with the O atom. Various combinations of these descriptors were assayed to estimate the O binding. Two criteria were carefully considered in constructing our models. The first one is the absence of multicollinearity; the highly correlated descriptors

are not considered in the model. The second one is omitting the combinations of variables that do not significantly contribute to the R^2 value. Thus, descriptors with p-values above 0.05 were rejected because they are not statistically significant.

As a result, the linear combination of two structural properties of Pt surfaces, average Pt−Pt distance of the NN, and the GCN of the atoms at the adsorption site led to an accurate description of the O binding energy on Pt surfaces. Figure 5b shows the relationship between the calculated and predicted O binding on Pt surfaces. For the model in (3), the R^2 value is 0.959 and the MAE is 0.087 eV, which is 4.8 and 5.2 times smaller than the MAEs when the d-band center and GCN are used as sole descriptors, respectively. Hence, the high R^2 and low MAE values are indicative of good model accuracy. Because the data sample of O atom interaction on Pt surfaces was limited, no model validation was performed. The predicted O binding energy, E_{bind}^{pred}, on Pt surfaces was estimated using the following model:

$$E_{bind}^{pred} = -5.395 - 0.344d_{Pt-Pt} + 0.271GCN \qquad (3)$$

where d_{Pt-Pt} and GCN are the average NN Pt−Pt distance and GCN of the atoms at the adsorption site, respectively. It is not surprising that these two properties are good descriptors of the O binding energy. It has been demonstrated that reactivity can be tuned by modifying the geometrical effects via the compression or expansion of the surface atoms. The adsorption properties of various monometallic surfaces have been manipulated when the surface atoms were under compressive and expansive strain.[8] Similarly, the effect of strain on the adsorption of O, OH, OOH, and CO on Pt and Au surfaces has been captured by a modified GCN.[37] Furthermore, the GCN, by definition, considers the differences between the adsorption sites.

The descriptors selected to decompose O binding on Pt nanoparticles were based on the structural and electronic features of isolated Pt nanoparticles. The five selected descriptors are the average NN Pt−Pt distance, GCN, sum of NN bond orders and their coordinating atoms, sum of NN + 2nd NN bond orders and their coordinating atoms, and the d-band centers of the atoms at the adsorption site. Several of these descriptors and combinations thereof may account for the changes in nanoparticle size and the various adsorption sites. In general, as the nanoparticle size increases, there is an expansion of interatomic distances, which is proportional to the effective nanoparticle radius.[38] However, large deviations from linearity have been observed for the interatomic distance of the surface atoms of Pt nanoparticles and their size.[18] For the ORR, the activity improves with increasing Pt nanoparticle size.[11,35] Geometrical and ligand effects have been shown to modify the activity[39] and stability of alloyed Pt nanoparticles.[40] Similarly, the GCN can account not only for the various adsorption sites but also for the nanoparticle size effect, as by definition, the GCN considers information about the coordination number of the 2nd NN. The GCN has been shown to be an indispensable descriptor of CO,[15] O atom, O_2, OOH, H_2O, and H_2O_2 adsorption on the top site of Pt nanoparticles.[14] Because individual bond orders and the sum of bond orders are directly related to the interatomic distance, bond orders can provide valuable information regarding stability and activity trends. It has been shown that as the Pt nanoparticle size increases, the average bond order of the surface atoms also increases.[18] In addition, the sum of bond

orders accounts for the interaction of all the atoms in the coordination sphere of the adsorption site, including those of the 3rd and 4th NNs. Thus, for the sum of NN and NN + 2nd NN bond orders, there is an overlapping or overcounting of the bond order for the same atom(s). It has been shown that as the Pt nanoparticle size increases, the d-band center of the entire nanoparticle decreases toward the bulk Pt value.[18] A similar tendency has been observed for the surface atoms of Pt nanoparticles converging to the d-band center value of Pt(111), although some deviations were reported for Pt_{201} and Pt_{405}.[18] Based on these descriptors, the model for predicting the binding energy of O on Pt nanoparticles is defined as follows:

$$E_{bind}^{pred} = -6.681 - 0.197d_{Pt-Pt} + 0.521GCN$$
$$+ 0.226BO^{NN} - 0.058BO^{NN+2^{nd}NN} - 0.427\varepsilon_d \qquad (4)$$

where BO^{NN}, $BO^{NN+2^{nd}NN}$, and ε_d are the sum of NN bond orders, sum of NN + 2nd NN bond orders, and the average d-band center of the NN of the adsorption site, respectively. Figure 5b illustrates the relationship between the DFT-calculated and predicted O binding energy, accounting for all the adsorption sites on Pt nanoparticles. The high R^2 (0.930) values indicate an excellent correlation between the predicted and DFT-calculated O binding energies. The MAE is 0.109 eV, which is 2.9 and 2.6 times lower than the d-band center and GCN alone as descriptors, respectively. Model validation was performed using the holdout method, wherein the data sample was randomly divided into two sets of data points: the training and test sets. The size of the training set was 3/4 of the data points in the sample, and the remaining 1/4 were assigned to the test set. Multiple regression analysis was performed on the training set, and the prediction model was used to estimate and validate the test set values. Ten different training and test sets were randomly selected. During the validation process, the descriptors were kept fixed to determine the prediction accuracy of the O binding energy. The coefficients of determination and the MAEs for the training and test sets of the 10 analyzed cases are shown in Table 1. The R^2 values for the test sets ranged from 0.847 to 0.969, and the MAEs ranged from 0.085 to 0.167 eV, confirming that the model is robust and appropriate for describing and predicting the O binding energy on Pt nanoparticles, as it considers the change in nanoparticle size and all possible adsorption sites. To the best

Table 1. Coefficients of Determination, R^2, and Mean Absolute Error (MAE) of the Training and Test Sets of O Binding on Pt Nanoparticles

case	R^2 training set	MAE (eV) training set	R^2 test set	MAE (eV) test set
1	0.940	0.112	0.847	0.105
2	0.926	0.113	0.879	0.102
3	0.949	0.097	0.898	0.167
4	0.931	0.098	0.925	0.154
5	0.915	0.108	0.942	0.124
6	0.920	0.109	0.947	0.133
7	0.928	0.099	0.957	0.147
8	0.911	0.115	0.962	0.092
9	0.907	0.118	0.964	0.085
10	0.904	0.113	0.969	0.097

of our knowledge, this is the first model wherein O binding energy was described, taking into consideration the Pt nanoparticle size effect and all the possible adsorption sites. The R^2 value between the calculated and predicted O binding energies on Pt nanoparticles obtained using eq 4 is significantly larger than the values obtained from the d-band center and GCN models (0.331 and 0.504, respectively).

When the same five descriptors were used to describe the O binding energy on Pt surfaces, R^2 was larger (0.976) than when using only two descriptors (0.959). However, not all the descriptors are statistically representative, and the AIC_C value was −0.779, which is much larger than when only two descriptors were used (−30.200). This is a result of a high degree of colinearity among some of the descriptors; for example, d_{Pt-Pt} with BO^{NN} and $BO^{NN+2^{nd}NN}$ and BO^{NN} with $BO^{NN+2^{nd}NN}$. Another possible model with statistically significant descriptors was obtained using a linear combination of the GCN and $BO^{NN+2^{nd}NN}$. These two descriptors have not only a lower R^2 value of 0.805 but also a higher AIC_C value (−17.715) compared to the linear combination of d_{Pt-Pt} and GCN. Thus, eq 3 is the simplest (lowest AIC_C) and most accurate equation for predicting the O binding energy (highest R^2). The differences between the descriptors used for surfaces and nanoparticles arise from the heterogeneity of the atoms in the outer Pt nanoparticle shell, which comprises vertex, ridge, and facet atoms, depending on the nanoparticle size.[18] Thus, the adsorption sites, consisting of these "unique atoms" and their combination, vary not only with the adsorption site type but also with increasing nanoparticle size. On the other hand, for pristine and homogeneous surfaces, the interatomic distance, coordination number, d-band center, and other parameters are identical for every surface atom. In addition, considering the coordination sphere of the adsorption site, the surface atoms have a coordination number of 7 for Pt(110), 8 for Pt(100), and 9 for Pt(111). In the case of nanoparticles, the surface atoms have a mixture of coordination numbers ranging from 5 to 9, which depends on the adsorption site type and nanoparticle size. Thus, fewer descriptors are required for characterizing O binding on surfaces than on nanoparticles.

From the absolute values of the standard partial regression coefficients, β, shown in Table 2, the most representative

Table 2. Descriptors for O Binding Energy on Pt Nanoparticles Only and Their Standard Partial Regression Coefficients, β

descriptor	β
d_{Pt-Pt}	−0.501
GCN	1.423
BO^{NN}	1.533
$BO^{NN+2^{nd}NN}$	−1.924
ε_d	−0.177

properties affecting the description of O atom interactions on Pt nanoparticles are those containing information about the NN and 2nd NN, in addition to considering the 3rd and 4th NN of the adsorption site atoms, that is, $BO^{NN+2^{nd}NN}$ followed by BO^{NN}. Next in importance is the GCN, which contains information about the NN and 2nd NN of the adsorption site. Finally, properties related only to the NN atoms, average Pt−Pt distance, and the d-band center have the least effect. Thus, to control nanoparticle activity, it is necessary to tune the

properties of not only the adsorption site atoms, but also their 2nd, 3rd, and 4th NNs. This information is crucial for the design of alloyed nanoparticles, wherein the ligand, ensemble, and geometrical effects directly affect the stability and activity.[40]

The same five descriptors used in eq 4 were selected to decompose the energetics of the O binding energy, considering the interaction of O on Pt nanoparticles and surfaces combined. The model is defined as follows:

$$E_{bind}^{pred} = -6.870 - 0.251d_{Pt-Pt} + 0.402GCN$$
$$+ 0.196BO^{NN} - 0.046BO^{NN+2^{nd}NN} - 0.654\varepsilon_d \tag{5}$$

Figure 5b depicts the relationship between the predicted and DFT-calculated O binding energies. The R^2 obtained with the use of eq 5 was 0.900, which is significantly larger than the values obtained when the d-band center or GCN was used as the sole descriptor (0.254 and 0.419, respectively). The MAE was 0.126 eV when eq 5 was employed to predict the O binding energy. The model was validated using the holdout method. The coefficients of determination and the MAEs for the training and test sets of the 10 analyzed cases are listed in Table 3. The R^2 values for the test set ranged from 0.791 to

Table 3. Coefficients of Determination, R^2, and Mean Absolute Error (MAE) for the Training and Test Sets Corresponding to O Binding on Pt Nanoparticles and Surfaces Combined

case	R^2 training set	MAE (eV) training set	R^2 test set	MAE (eV) test set
1	0.912	0.126	0.791	0.134
2	0.957	0.119	0.839	0.163
3	0.908	0.116	0.840	0.148
4	0.918	0.111	0.853	0.185
5	0.896	0.132	0.879	0.120
6	0.898	0.123	0.900	0.112
7	0.910	0.125	0.904	0.154
8	0.896	0.132	0.912	0.131
9	0.901	0.131	0.916	0.138
10	0.894	0.119	0.934	0.163

0.934, indicating that good accuracy is to be expected when using the proposed model to estimate O binding energies on Pt surfaces and Pt nanoparticles. The range of the MAEs corresponding to the test sets (0.112−0.185 eV) slightly increased compared to the case of only nanoparticles but was much smaller than a single descriptor predicting the O binding energy. eq 5 represents the first O binding energy model that takes into consideration nanoparticle size effects and the various adsorption site types on nanoparticles and Pt surfaces. Table 4 summarizes the β values of the five descriptors used to estimate the O binding energy on Pt surfaces and nanoparticles combined. The absolute values of β given in Table 4 indicate that the degree of representation by the Pt surface and nanoparticle properties follow the same trend as in the Pt nanoparticle case. Although this was expected because of the 5.5:1 ratio of data values for the O binding energy on Pt nanoparticles vs Pt surfaces, there is a considerable decrease in the absolute value of β for the descriptors that contain information encompassing NN atoms, that is, the $BO^{NN+2^{nd}NN}$, BO^{NN}, and GCN. On the other hand, β values for average Pt−

Table 4. Descriptors of O Binding Energy on Pt Surfaces and Nanoparticles and Their Standard Partial Regression Coefficients, β

descriptor	β
d_{Pt-Pt}	−0.643
GCN	1.115
BO^{NN}	1.317
$BO^{NN + 2^{nd} NN}$	−1.523
ε_d	−0.250

Pt distances and the *d*-band center of NN atoms increased. Surface reconstruction phenomena may occur for clean surfaces and have been of great interest to surface science. Of particular importance to catalysis are surface reconstructions induced by adsorbates.[41,42] For Pt surfaces, Pt(110) suffered reconstruction and distortion due to the interaction of O atoms at high coverages.[33,43] DFT calculations showed the deformation of Pt nanoparticles with 1 ML oxygen coverage.[44] In this study, the interaction of a single O atom with Pt surfaces and nanoparticles is investigated. No major reconstructions were observed after O chemisorption. One limitation of our predicting models is that they cannot be used if significant distortions occur after the O interaction with the Pt nanoparticles. However, to corroborate this limitation, more calculations are required.

CONCLUSIONS

Detailed analysis of geometrical, electronic, and chemical properties of Pt nanoparticles and Pt surfaces confirmed that neither the *d*-band center nor the GCN can be used as the sole descriptor to predict the O binding energy on Pt nanoparticles or Pt surfaces. Multiple regression analysis was performed to describe the O binding energy on Pt surfaces only, on Pt nanoparticles only, and on all the possible adsorption sites on Pt surfaces and Pt nanoparticles; in each case, the proposed model was more accurate than the conventional models in predicting the O binding energy. In the case of O binding on Pt surfaces, interaction energetics were described using two structural properties of pristine surfaces. The model provided an excellent correlation with the DFT-calculated adsorption energies. The proposed model of O binding on Pt nanoparticles employs a linear combination of five descriptors acquired from the structural and electronic properties of Pt nanoparticles. Model validation confirmed its accuracy and robustness in estimating the O binding energy. Finally, an O binding energy model that considers not only the nanoparticle size effects, but also all the possible adsorption sites of Pt surfaces and nanoparticles is proposed for the first time. The model provides a good linear fit, and its validation confirms that the model performs well in describing the chemisorption of O atoms on Pt surfaces and Pt nanoparticles.

AUTHOR INFORMATION

Corresponding Author

Michihisa Koyama − *Department of Hydrogen Energy Systems, Graduate School of Engineering and INAMORI Frontier Research Center, Kyushu University, Fukuoka 819-0395, Japan; Center for Green Research on Energy and Environmental Materials, National Institute for Materials Science, Ibaraki 305-0044, Japan; Research Initiative for Supra-Materials, Shinshu University, Nagano 380-8553, Japan; Graduate School of Advanced Engineering and Science, Hiroshima University, Hiroshima 739-8527, Japan; Open Innovation Institute, Kyoto University, Kyoto 606-8501, Japan*; Email: koyama_michihisa@shinshu-u.ac.jp, koyama.michihisa.5k@kyoto-u.ac.jp

Authors

David S. Rivera Rocabado − *Department of Hydrogen Energy Systems, Graduate School of Engineering, Kyushu University, Fukuoka 819-0395, Japan; Graduate School of Nanobioscience, Yokohama City University, Yokohama, Kanagawa 236-0027, Japan; Center for Green Research on Energy and Environmental Materials, National Institute for Materials Science, Ibaraki 305-0044, Japan;* orcid.org/0000-0002-4691-3433

Yusuke Nanba − *INAMORI Frontier Research Center, Kyushu University, Fukuoka 819-0395, Japan; Center for Green Research on Energy and Environmental Materials, National Institute for Materials Science, Ibaraki 305-0044, Japan; Research Initiative for Supra-Materials, Shinshu University, Nagano 380-8553, Japan;* orcid.org/0000-0002-1692-4465

Complete contact information is available at:
https://pubs.acs.org/10.1021/acsomega.1c01726

Notes

The authors declare no competing financial interest.

ACKNOWLEDGMENTS

REFERENCES

(1) Greeley, J.; Stephens, I. E. L.; Bondarenko, A. S.; Johansson, T. P.; Hansen, H. A.; Jaramillo, T. F.; Rossmeisl, J.; Chorkendorff, I.; Nørskov, J. K. Alloys of Platinum and Early Transition Metals as Oxygen Reduction Electrocatalysts. *Nat. Chem.* **2009**, *1*, 552−556.

(2) Kulkarni, A.; Siahrostami, S.; Patel, A.; Nørskov, J. K. Understanding Catalytic Activity Trends in the Oxygen Reduction Reaction. *Chem. Rev.* **2018**, *118*, 2302−2312.

(3) Krüger, S.; Vent, S.; Rösch, N. Size Dependence of Bond Length and Binding Energy in Palladium and Gold Clusters. *Ber. Bunsenges. Phys. Chem.* **1997**, *101*, 1640−1643.

(4) Hammer, B.; Nørskov, J. K. Theoretical Surface Science and Catalysis—Calculations and Concepts. In *Advances in Catalysis*; Elsevier, 2000; Vol. 45, pp. 71−129.

(5) Lu, C.; Lee, I. C.; Masel, R. I.; Wieckowski, A.; Rice, C. Correlations between the Heat of Adsorption and the Position of the Center of the d-Band: Differences between Computation and Experiment. *J. Phys. Chem. A* **2002**, *106*, 3084−3091.

(6) Kim, G.; Kawazoe, Y.; Lee, K.-R. Controlled Catalytic Properties of Platinum Clusters on Strained Graphene. *J. Phys. Chem. Lett.* **2012**, *3*, 1989−1996.

(7) Greeley, J.; Nørskov, J. K. A General Scheme for the Estimation of Oxygen Binding Energies on Binary Transition Metal Surface Alloys. *Surf. Sci.* **2005**, *592*, 104−111.

(8) Mavrikakis, M.; Hammer, B.; Nørskov, J. K. Effect of Strain on the Reactivity of Metal Surfaces. *Phys. Rev. Lett.* **1998**, *81*, 2819−2822.

(9) Stamenkovic, V.; Mun, B. S.; Mayrhofer, K. J. J.; Ross, P. N.; Markovic, N. M.; Rossmeisl, J.; Greeley, J.; Nørskov, J. K. Changing the Activity of Electrocatalysts for Oxygen Reduction by Tuning the

Surface Electronic Structure. *Angew. Chem., Int. Ed.* **2006**, *45*, 2897−2901.

(10) Jiang, T.; Mowbray, D. J.; Dobrin, S.; Falsig, H.; Hvolbæk, B.; Bligaard, T.; Nørskov, J. K. Trends in CO Oxidation Rates for Metal Nanoparticles and Close-Packed, Stepped, and Kinked Surfaces. *J. Phys. Chem. C* **2009**, *113*, 10548−10553.

(11) Han, B. C.; Miranda, C. R.; Ceder, G. Effect of Particle Size and Surface Structure on Adsorption of O and OH on Platinum Nanoparticles: A First-Principles Study. *Phys. Rev. B* **2008**, *77*, No. 075410.

(12) Takigawa, I.; Shimizu, K.; Tsuda, K.; Takakusagi, S. Machine Learning Predictions of Factors Affecting the Activity of Heterogeneous Metal Catalysts. In *Nanoinformatics*; Tanaka, I., Ed.; Springer Singapore: Singapore, 2018; pp. 45−64.

(13) Mpourmpakis, G.; Andriotis, A. N.; Vlachos, D. G. Identification of Descriptors for the CO Interaction with Metal Nanoparticles. *Nano Lett.* **2010**, *10*, 1041−1045.

(14) Calle-Vallejo, F.; Martínez, J. I.; García-Lastra, J. M.; Sautet, P.; Loffreda, D. Fast Prediction of Adsorption Properties for Platinum Nanocatalysts with Generalized Coordination Numbers. *Angew. Chem., Int. Ed.* **2014**, *53*, 8316−8319.

(15) Gasper, R.; Shi, H.; Ramasubramaniam, A. Adsorption of CO on Low-Energy, Low-Symmetry Pt Nanoparticles: Energy Decomposition Analysis and Prediction via Machine-Learning Models. *J. Phys. Chem. C* **2017**, *121*, 5612−5619.

(16) Nanba, Y.; Koyama, M. NO Adsorption on 4d and 5d Transition-Metal (Rh, Pd, Ag, Ir, and Pt) Nanoparticles: Density Functional Theory Study and Supervised Learning. *J. Phys. Chem. C* **2019**, *123*, 28114−28122.

(17) Nanba, Y.; Koyama, M. An Element-Based Generalized Coordination Number for Predicting the Oxygen Binding Energy on Pt_3M (M = Co, Ni, or Cu) Alloy Nanoparticles. *ACS Omega* **2021**, *6*, 3218−3226.

(18) Rivera Rocabado, D. S.; Ishimoto, T.; Koyama, M. The Effect of $SnO_2(110)$ Supports on the Geometrical and Electronic Properties of Platinum Nanoparticles. *SN Appl. Sci.* **2019**, *1*, 1485.

(19) Kresse, G.; Hafner, J. Ab Initio Molecular Dynamics for Liquid Metals. *Phys. Rev. B: Condens. Matter. Phys.* **1993**, *47*, 558−561.

(20) Kresse, G.; Furthmüller, J. Efficient Iterative Schemes for Ab Initio Total-Energy Calculations Using a Plane-Wave Basis Set. *Phys. Rev. B: Condens. Matter. Phys.* **1996**, *54*, 11169−11186.

(21) Kresse, G.; Furthmüller, J. Efficiency of Ab-Initio Total Energy Calculations for Metals and Semiconductors Using a Plane-Wave Basis Set. *Comput. Mater. Sci.* **1996**, *6*, 15−50.

(22) Blöchl, P. E. Projector Augmented-Wave Method. *Phys. Rev. B: Condens. Matter. Phys.* **1994**, *50*, 17953−17979.

(23) Arblaster, J. W. Crystallographic Properties of Platinum. *Platinum Met. Rev.* **1997**, *41*, 12−21.

(24) Manz, T.; Introducing, A. DDEC6 Atomic Population Analysis: Part 3. Comprehensive Method to Compute Bond Orders. *RSC Adv.* **2017**, *7*, 45552−45581.

(25) Akaike, H. Information Theory and an Extension of the Maximum Likelihood Principle, In *Selected Papers of Hirotugu Akaike*, Parzen, E., Tanabe, K., Kitagawa, G. (Eds.). Springer Series in Statistics (Perspectives in Statistics). Springer, New York, NY; 1998; pp. 199−213.

(26) Hurvich, C. M.; Tsai, C.-L. Regression and Time Series Model Selection in Small Samples. *Biometrika* **1989**, *76*, 297−307.

(27) Xin-She, Y. *Introduction to Algorithms for Data Mining and Machine Learning*; Elsevier, 2019.

(28) Burnham, K. P.; Anderson, D. R. *Model Selection and Multimodel Inference*; Burnham, K. P., Anderson, D. R., Eds.; Springer New York: New York, NY, 2004.

(29) Materer, N.; Starke, U.; Barbieri, A.; Döll, R.; Heinz, K.; Van Hove, M. A.; Somorjai, G. A. Reliability of Detailed LEED Structural Analyses: Pt(111) and Pt(111)-p(2×2)-O. *Surf. Sci.* **1995**, *325*, 207−222.

(30) Yeo, Y. Y.; Vattuone, L.; King, D. A. Calorimetric Heats for CO and Oxygen Adsorption and for the Catalytic CO Oxidation Reaction on Pt{111}. *J. Chem. Phys.* **1997**, *106*, 392−401.

(31) Parker, D. H.; Bartram, M. E.; Koel, B. E. Study of High Coverages of Atomic Oxygen on the Pt(111) Surface. *Surf. Sci.* **1989**, *217*, 489−510.

(32) Narayanan, R.; El-Sayed, M. A. Shape-Dependent Catalytic Activity of Platinum Nanoparticles in Colloidal Solution. *Nano Lett.* **2004**, *4*, 1343−1348.

(33) Gai, L.; Shin, Y. K.; Raju, M.; van Duin, A. C. T.; Raman, S. Atomistic Adsorption of Oxygen and Hydrogen on Platinum Catalysts by Hybrid Grand Canonical Monte Carlo/Reactive Molecular Dynamics. *J. Phys. Chem. C* **2016**, *120*, 9780−9793.

(34) Shao, M.; Peles, A.; Shoemaker, K. Electrocatalysis on Platinum Nanoparticles: Particle Size Effect on Oxygen Reduction Reaction Activity. *Nano Lett.* **2011**, *11*, 3714−3719.

(35) Mayrhofer, K. J. J.; Blizanac, B. B.; Arenz, M.; Stamenkovic, V. R.; Ross, P. N.; Markovic, N. M. The Impact of Geometric and Surface Electronic Properties of Pt-Catalysts on the Particle Size Effect in Electrocatalysis. *J. Phys. Chem. B* **2005**, *109*, 14433−14440.

(36) Ouyang, R.; Curtarolo, S.; Ahmetcik, E.; Scheffler, M.; Ghiringhelli, L. M. SISSO: A Compressed-Sensing Method for Identifying the Best Low-Dimensional Descriptor in an Immensity of Offered Candidates. *Phys. Rev. Mater.* **2018**, *2*, No. 083802.

(37) Calle-Vallejo, F.; Bandarenka, A. S. Enabling Generalized Coordination Numbers to Describe Strain Effects. *ChemSusChem* **2018**, *11*, 1824−1828.

(38) Roduner, E. Size Matters: Why Nanomaterials Are Different. *Chem. Soc. Rev.* **2006**, *35*, 583−592.

(39) Strasser, P.; Koh, S.; Anniyev, T.; Greeley, J.; More, K.; Yu, C.; Liu, Z.; Kaya, S.; Nordlund, D.; Ogasawara, H.; et al. Lattice-Strain Control of the Activity in Dealloyed Core−Shell Fuel Cell Catalysts. *Nat. Chem.* **2010**, *2*, 454−460.

(40) Rivera Rocabado, D. S.; Nanba, Y.; Koyama, M. Electronic Structure and Phase Stability of Pt_3M (M = Co, Ni, and Cu) Bimetallic Nanoparticles. *Comput. Mater. Sci.* **2020**, *184*, No. 109874.

(41) Kolb, D. Reconstruction Phenomena at Metal-Electrolyte Interfaces. *Prog. Surf. Sci.* **1996**, *51*, 109−173.

(42) Sharma, R.; Brown, W.; King, D. The Adsorption of CO on Pt{110} over the Temperature Range from 90 to 300K Studied by RAIRS. *Surf. Sci.* **1998**, *414*, 68−76.

(43) Zhu, T.; Sun, S.-G.; van Santen, R. A.; Hensen, E. J. M. Reconstruction of Clean and Oxygen-Covered Pt(110) Surfaces. *J. Phys. Chem. C* **2013**, *117*, 11251−11257.

(44) Verga, L. G.; Aarons, J.; Sarwar, M.; Thompsett, D.; Russell, A. E.; Skylaris, C.-K. DFT Calculation of Oxygen Adsorption on Platinum Nanoparticles: Coverage and Size Effects. *Faraday Discuss.* **2018**, *208*, 497−522.